Journal of Power Sources 245 (2014) 624–629

Contents lists available at SciVerse ScienceDirect

Journal of Power Sources

journal homepage: www.elsevier.com/locate/jpowsour

Gold coating for a high performance $Li_4Ti_5O_{12}$ nanorod aggregates anode in lithium-ion batteries

Wei Wang [a], Yuanyuan Guo [a], Lixiang Liu [a], Shixiong Wang [a], Xiangjun Yang [a], Hong Guo [a,b,*]

[a] School of Chemistry Science and Engineering, Yunnan University, No. 2, Green Lake North Road, Kunming 650091, Yunnan, China
[b] School of Chemistry and Chemical Engineering, Qujing Normal University, Qujing 655000, Yunnan, China

HIGHLIGHTS

- Au@LTO nanorod aggregates are synthesized through a facile route.
- Au@LTO possesses high BET surface area and enhanced lithium diffusion coefficient.
- As-prepared Au@LTO exhibits superior rate capacity and stability.

GRAPHICAL ABSTRACT

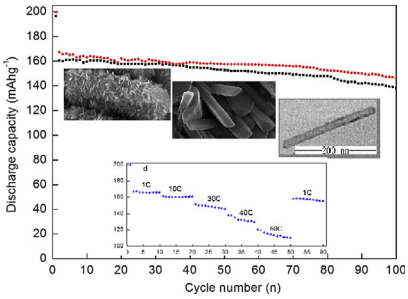

ARTICLE INFO

Article history:
Received 8 April 2013
Received in revised form
26 June 2013
Accepted 27 June 2013
Available online 5 July 2013

Keywords:
$Li_4Ti_5O_{12}$
Nanorod
High rate
Li-ion batteries

ABSTRACT

An effective strategy by combination of alcoholysis, solid-state reaction and coating techniques is employed to prepare Au@$Li_4Ti_5O_{12}$ nanorod aggregates as anode materials for Li-ion batteries. The lithium diffusion coefficient of resulting Au@$Li_4Ti_5O_{12}$ is 7.32×10^{-10} cm^2 s^{-1}, and its stable reversible capacity is 169 mAh g^{-1} with the retention of 91.1% after 100 cycles at 5 C. Moreover, it also exhibits excellent rate-capability performance. The superior cycling performance can be attributed to the unique nanorod characteristics, structural stability, and the improved ionic and electronic conduction in the electrode due to the uniform nano coating of Au.

1. Introduction

Rechargeable lithium-ion batteries have long been considered to be one of the most promising energy storage systems because of the higher energy density, higher rate, higher stability, longer cycle life, and improved safety than competing batteries [1–3]. Intensive worldwide attempts have been focused on lithium titanate oxide ($Li_4Ti_5O_{12}$) materials due to its zero-strain characteristic and high insertion potential of 1.55 V vs Li^+/Li during lithium insertion/extraction. Additionally, $Li_4Ti_5O_{12}$ has no solid–electrolyte interface, which allows the electrode to meet the high power and abuse tolerance requirements needed for power sources [4–7]. However, $Li_4Ti_5O_{12}$ still exhibits poor lithium storage properties at high current rates owing to the low electronic conductivity (ca. 10^{-13} S cm^{-1}) and lithium diffusion coefficient (ca. 10^{-13} cm^2 s^{-1}) [8–10]. Large improvements have been focused on improving the electronic conductivity and electrochemical properties by using various doping,

* Corresponding author. School of Chemistry Science and Engineering, Yunnan University, Kunming 650091, Yunnan, China. Tel.: +86 871 65032180.
E-mail address: guohongcom@126.com (H. Guo).

0378-7753/$ – see front matter © 2013 Elsevier B.V. All rights reserved.
http://dx.doi.org/10.1016/j.jpowsour.2013.06.156

mixing, coating techniques, and nano-sized $Li_4Ti_5O_{12}$ particles with various morphologies [11–16]. These materials have been proven to exhibit better electrochemical performance, suggesting that structure modification and coating techniques could be the effective solutions to enhance the electrochemical performance. Compared with conventional methods produced nanostructured $Li_4Ti_5O_{12}$ and carbon coating route, reports on large scale synthesis of nanorod $Li_4Ti_5O_{12}$ anodes are quite rare. Furthermore, the previous efforts show that noble metal additives can increase electronic conductivity of electrode greatly and improved its high-rate discharge capacity and cycling stability obviously compared with carbon hybrid materials [17–21]. For instance, Wen and co-workers synthesized $Li_4Ti_5O_{12}$/Ag materials, which can be used as high capacity anodes for lithium ion batteries [17,18]. Wang and co-workers fabricated mesoporous Au/$Li_4Ti_5O_{12}$ spheres with high rate capability [21].

Herein, a new strategy to synthesize Au@$Li_4Ti_5O_{12}$ nanorod aggregates with enhanced lithium storage combining solvother mal alcoholysis and solid-state reaction in large quantities is proposed in this work. It is based on the following understandings: Firstly, 3D flower-like TiO_2 nanorod formed during the course of solvothermal alcoholysis, and then $Li_4Ti_5O_{12}$ nanorod was produced after calcinations of the as-prepared TiO_2 and Li_2CO_3 composites at 800 °C for 10 h. Subsequent coating technique of the LTO materials resulted in the formation of Au@$Li_4Ti_5O_{12}$ nanorod aggregates. Compared with conventional methods for preparation of $Li_4Ti_5O_{12}$ nano materials, the Au@$Li_4Ti_5O_{12}$ materials prepared as such have relatively higher surface area and stable 2D nanorod configuration. The former can render much contact area between active materials and Li-ion in the process of electrochemical reaction, and the latter can shorten path lengths for Li-ion transport. In particular, the coating of Au can enhance the electronic conductivity. All the factors will contribute greatly to the high specific capacity, high rate capacity and good cycling performance of $Li_4Ti_5O_{12}$ anodes. The structure and electrochemical performance of synthesized Au@$Li_4Ti_5O_{12}$ nanorods materials are investigated primarily.

2. Experimental

2.1. Synthesis of 3D flower-like TiO_2

All the reagents are of analytical grade and are used without further purification. To synthesize the 3D flower-like TiO_2. In a typical synthesis, 0.391 g of titanium (IV) oxysulfate–sulfuric acid hydrate and 36 mL ethanol at room temperature with stirring for 10 min, followed by addition of 16.6 mL of glycerol and 16.4 mL of ethyl ether, the mixture was kept stirring for 30 min, the suspension was transferred into in 80 mL Teflon-lined stainless autoclave and heated to a temperature of 110 °C for 48 h. After the autoclave cooled to room temperature, the product was collected by centrifugation, and then washed with deionized water and ethanol several times. Subsequently it was dried at 60 °C for 6 h, and calcined at 550 °C for 4 h to remove the residual organics. Finally a white precipitate was harvested.

2.2. Synthesis of $Li_4Ti_5O_{12}$ nanorod aggregates

Virginal $Li_4Ti_5O_{12}$ nanorod aggregates were synthesized by solid-state reaction. Stoichiometric amount of TiO_2 and Li_2CO_3 (nLi:nTi = 0.8) were mixed by grinding method for 10 h, and then the as-prepared powder was calcined at 800 °C for 10 h in air.

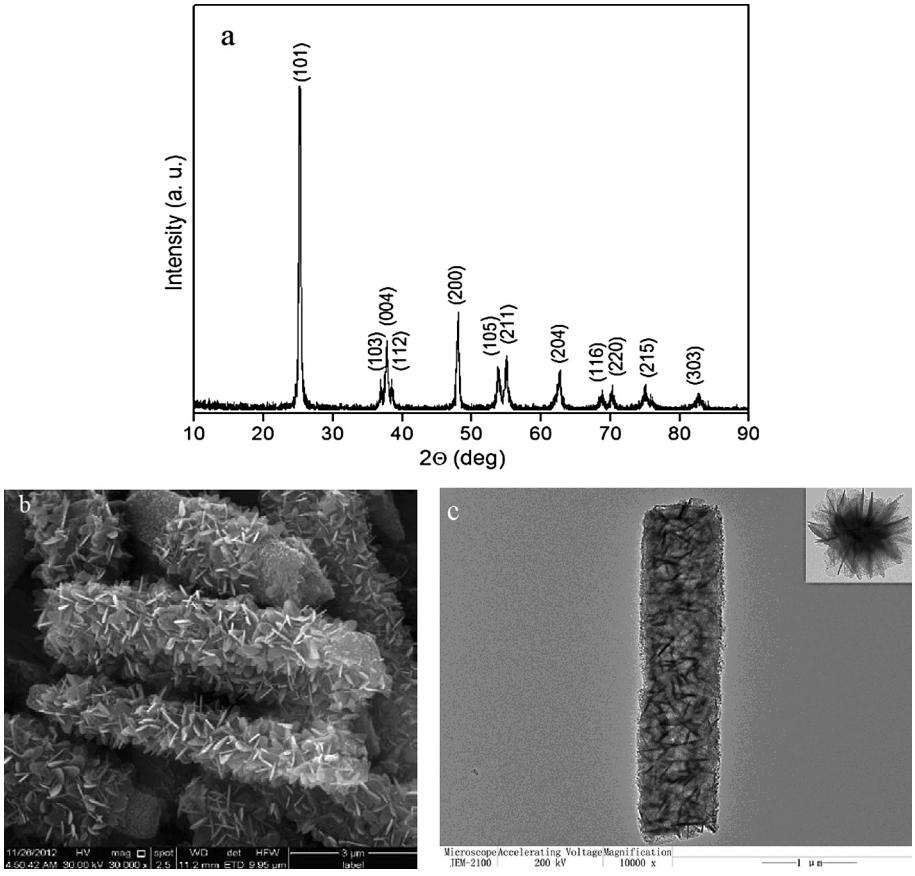

Fig. 1. (a) XRD pattern, SEM (b) and TEM (c) micrograph of the as-synthesized 3D flower-like TiO_2. The inset in (c) is a single partially broken particle.

2.3. Synthesis of Au@$Li_4Ti_5O_{12}$ nanorod aggregates

The Au@$Li_4Ti_5O_{12}$ nanorods were prepared through the following method. For a typical procedure: 0.1193 g of $Li_4Ti_5O_{12}$ was added to mixed solution of EG and PVP under stirring. The solution was heated and kept at 170 °C, and followed by addition of 15 mL of 1 g L^{-1} Au (III) solution, drop-by-drop. The mixture was stirred for 4 h. The precipitate was harvested by centrifugation and washing with deionized water and ethanol for three times. The obtained product was dried in air at 60 °C for 6 h and calcined at 550 °C for 4 h to form final products.

Characterization: X-ray diffraction (XRD) was carried out to identity the phase composition of synthesized samples over the 2θ range from 20° to 90° using a Rigaku D/max-A diffractometer with Co Kα radiation. Morphologies of the synthesized TiO_2 and Au@$Li_4Ti_5O_{12}$ samples were observed with a AMRAY 1000B scanning electron microscope (SEM), and the microstructural characteristics of LTO nanorods were observed by high-resolution transmission electron microscope (HR-TEM, JEOL JEM-2010) working at 200 kV accelerating voltage and the lattice structure was identified by selected area electron diffraction (SAED) technique. BET surface areas, and pore volumes were measured by nitrogen adsorption/desorption using a NOVA 2000e gas sorption analyzer (Quantachrome Corp).

Electrochemical measurements: For electrochemical performance evaluation, half-cell studies were performed. In the experimental LTO electrode, acetylene black powder and polyvinylidene fluoride (PVDF) were used as conductive additive and binder. The synthesized LTO nanorods were mixed with acetylene black and PVDF dissolved in *N*-methyl-pyrrolidinone in the weight ratio of 80:10:10 to form slurry, which was painted on a copper foil used as current collector. After solvent evaporation, the electrode was pressed and

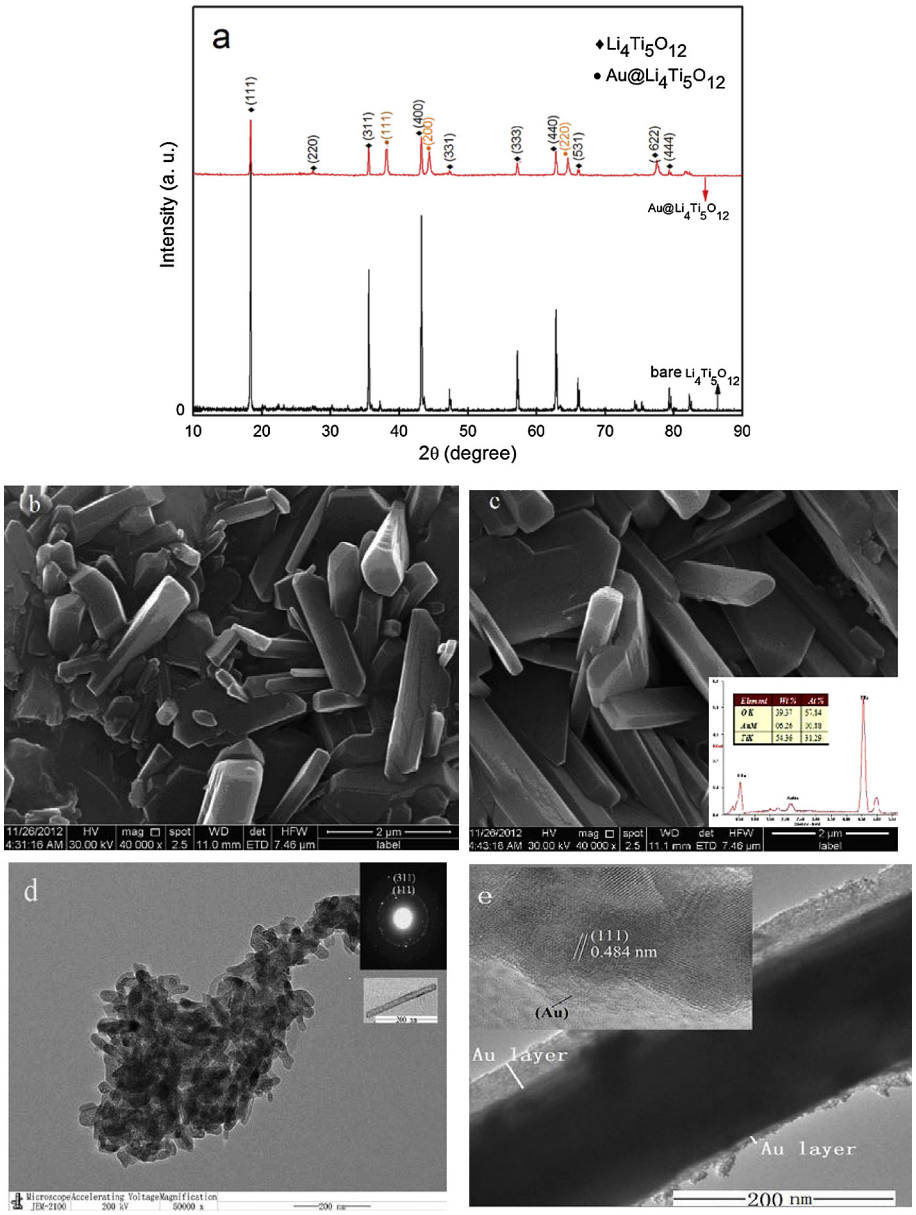

Fig. 2. (a) XRD pattern of bare $Li_4Ti_5O_{12}$ and Au@ $Li_4Ti_5O_{12}$. SEM micrograph of the prepared $Li_4Ti_5O_{12}$ (b) and Au@ $Li_4Ti_5O_{12}$ (c) nanorod aggregates. TEM micrographs (d) and (e) of Au@$Li_4Ti_5O_{12}$ nanorod aggregates at different magnifications. The insets in (d) are the selected area electron diffraction and TEM micrograph of a single nanorod. The inset in Fig. 2e is HRTEM morphology of Au@LTO structure corresponding to spinel $Li_4Ti_5O_{12}$ (1 1 1) plane spacing.

dried at 120 °C under vacuum for 48 h. The cells were assembled in argon filled glove-box. Metallic lithium foil was used as counter electrode. The electrolyte was 1 M $LiPF_6$ in a mixture of ethylene carbonate (EC) and dimethyl carbonate (DMC) (1:1 in vol. ratio). Cycling tests were carried out in the voltage range of 1.0–2.5 V versus Li/Li^+ by Land 2100A tester. Cyclic voltammetry was performed by CHI660D electrochemical workstation between 1.0 and 2.5 V at scan rate of 0.05 mV s^{-1}.

3. Results and discussion

Characterizations shown as the XRD pattern of the synthesized materials (Fig. 1a) declare that the product displays a tetragonal anatase TiO_2 structure (JCPDS card No. 21-1272, $a = 0.3789$ nm, $c = 0.9154$ nm). Detailed analysis of the peak broadening of the (1 0 1) reflection using the Scherrer equation indicates an average crystallite size ca. 7 nm, suggesting that the anatase TiO_2 particles are composed of nanocrystal subunits. Fig. 1b and c is SEM and TEM images of prepared TiO_2 nanorods yielded by solvothermal alcoholysis and subsequent calcinations at 550 °C. It illuminates the synthesized powders are uniform 3D flower-like rod shape with diameter of ca. 1.5 μm. It is interesting to find that the inner parts of TiO_2 exhibit rod structure, while its surface is assembled by nano sheets with thickness of ca. 5 nm as evidenced by Fig. 1c. Observation on a single partially broken particle, as shown in the inset in Fig. 1c, also indicates the nanorod is made up from thin nano sheet.

The phase structure of the as-synthesized $Li_4Ti_5O_{12}$ and $Au@Li_4Ti_5O_{12}$ samples is characterized using power X-ray diffraction as shown in Fig. 2a. All these peaks can be indexed as spinel lithium titanate (JCPDS card No. 49-0207) for bare $Li_4Ti_5O_{12}$ sample. The acutance of the diffraction peaks is ascribed to high crystalline of the material. No other peaks such as TiO_2 are detected, indicating the purity of the $Li_4Ti_5O_{12}$ product. Compared with $Li_4Ti_5O_{12}$, the XRD of $Au@Li_4Ti_5O_{12}$ detected the peaks attributed to Au obviously, suggesting the Au is successful coated on the surfaces of the $Li_4Ti_5O_{12}$. According to SEM images of the $Li_4Ti_5O_{12}$ and $Au@Li_4Ti_5O_{12}$ as shown in Fig. 2b and c, the morphology of $Li_4Ti_5O_{12}$ and $Au@Li_4Ti_5O_{12}$ are similar to each other. It indicates the prepared $Au@Li_4Ti_5O_{12}$ kept the original structure of $Li_4Ti_5O_{12}$ without destruction. Both of them exhibit rod structures with diameter not much than 1 μm, which is a little shrinkage in size than that of as-synthesized TiO_2 rods. The EDX analysis (inset in Fig. 2c) detects some Au on the surface of $Li_4Ti_5O_{12}$, which is agreement with XRD results.

To further examine the architecture of the $Au@Li_4Ti_5O_{12}$, the samples are investigated by TEM and HRTEM as shown in Fig. 2d and e. It can be clearly distinguished that the samples of $Au@Li_4Ti_5O_{12}$ are nanorods aggregates, and the diameter of a single nanorod is estimated to be 10–20 nm. Its selected-area electron diffraction (SAED) pattern (Fig. 2d inset) reveals the diffraction rings are indexed to (1 1 1), and (3 1 1) diffraction of spinel $Li_4Ti_5O_{12}$, respectively, which indicates that the $Li_4Ti_5O_{12}$ nanocage is composed of fine crystal particles with partial orientation. The highly crystallized spinel phase can greatly improve the crystallographic structure stability and charge–discharge ability of $Li_4Ti_5O_{12}$ [22,23]. Because the electrode reaction depends on both ionic and electronic conductivity and decreasing the particle size can only improve the ionic conductivity of electrode, so Au coating strategy is adopted to enhance the electronic conduction of the electrode with the aim of improving further the rate capability. Fig. 2e reveals that the nano-sized particle has actually Au coated structure, which is composed of a crystal structure phase and the Au layer on the surface. The lattice spacing (0.484 nm) agrees with spinel $Li_4Ti_5O_{12}$ (1 1 1) plane spacing. The Au layer with the thickness ranging from 4 nm to 70 nm can be clearly observed on the particle surface, which confirms the analysis of XRD and EDX. The coating of Au is expected to be favorable for the enhancement of electronic conductivity and thus the rate capability of electrode.

Fig. 3 shows the N_2 adsorption/desorption isotherms and the pore size distribution of the $Au@Li_4Ti_5O_{12}$ sample. The isotherms are identified as type IV. The pore size distribution data indicates that a majority of the pores are smaller than 25 nm. The BET surface area of the sample is 50.35 m^2 g^{-1}. The single point total volume of pores at $P/P_0 = 0.975$ is 0.23 cm^3 g^{-1}. The BET surface area and the large total pore volume strongly indicate that the prepared $Li_4Ti_5O_{12}$ nanorod aggregates are a loose structure in fact. This structure can not only keep the nano effect of electrode but can help to enlarge contact area between active $Li_4Ti_5O_{12}$ and Li ion in the process of electrochemical reaction.

The electrochemical performance of the $Li_4Ti_5O_{12}$ and $Au@Li_4Ti_5O_{12}$ nanorod aggregates used for Li-ion anodic materials is investigated. The cycling performance profiles of $Li_4Ti_5O_{12}$ and $Au@Li_4Ti_5O_{12}$ electrodes at constant current density of 5 C are shown in Fig. 4a. The initial reversible capacities are 194 and 199 mAh g^{-1} for bare $Li_4Ti_5O_{12}$ and $Au@Li_4Ti_5O_{12}$ with corresponding coulombic efficiencies of 81.6 and 85.3%, respectively. The stable reversible capacity of electrode is 169 mAh g^{-1}, and can be retained at 154 mAh g^{-1} after 100 cycles with the retention of 91.1%. The coulombic efficiencies are always over 99.3% except for the first cycle at 5 C. While the bare $Li_4Ti_5O_{12}$ samples present only 135 mAh g^{-1} after 100 cycles. Hence, $Au@Li_4Ti_5O_{12}$ exhibits improved reversibility. Cyclic voltammetry plots of $Au@Li_4Ti_5O_{12}$ and bare $Li_4Ti_5O_{12}$ electrode are shown as Fig. 4b, which reveals that the polarization is decreased after Au coating. The CV plots of the obtained $Au@Li_4Ti_5O_{12}$ electrode for the 1st, 2nd and 100th cycle are shown in Fig. 4c. The cathodic/anodic peaks located at c.a. 1.38 and 1.75 V are associated with lithium insertion/extraction in the spinel lattice, which is a little difference with other research groups [12,24,25]. The difference is mainly attributed to the lithium ion diffusivity rate verifying in various spinels $Li_4Ti_5O_{12}$ with different morphology and microstructure. The CV curves become almost overlapping for the 2nd and 100th cycle, suggesting the excellent cycling stability of $Au@Li_4Ti_5O_{12}$ electrode.

To understand the improved high-rate performance after introducing conducting Au into $Li_4Ti_5O_{12}$, The electronic conductivity and electrochemical impedance spectroscopy are measured. The electronic conductivity of $Au@Li_4Ti_5O_{12}$ hybrid materials (ca.

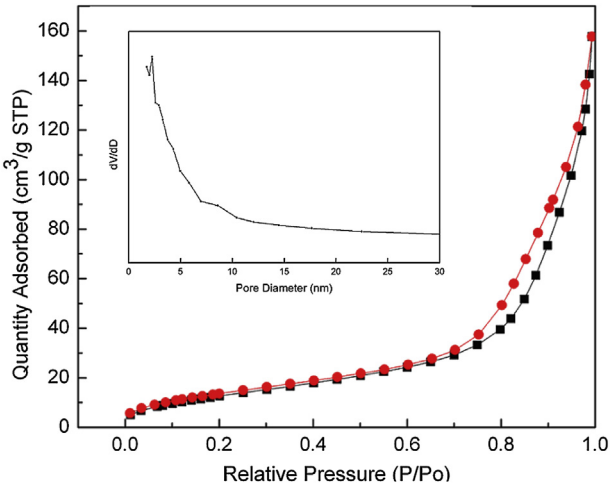

Fig. 3. Nitrogen adsorption/desorption isotherm and Barrett–Joyner–Halenda (BJH) pore size distribution plot (inset) of the prepared $Au@Li_4Ti_5O_{12}$ sample.

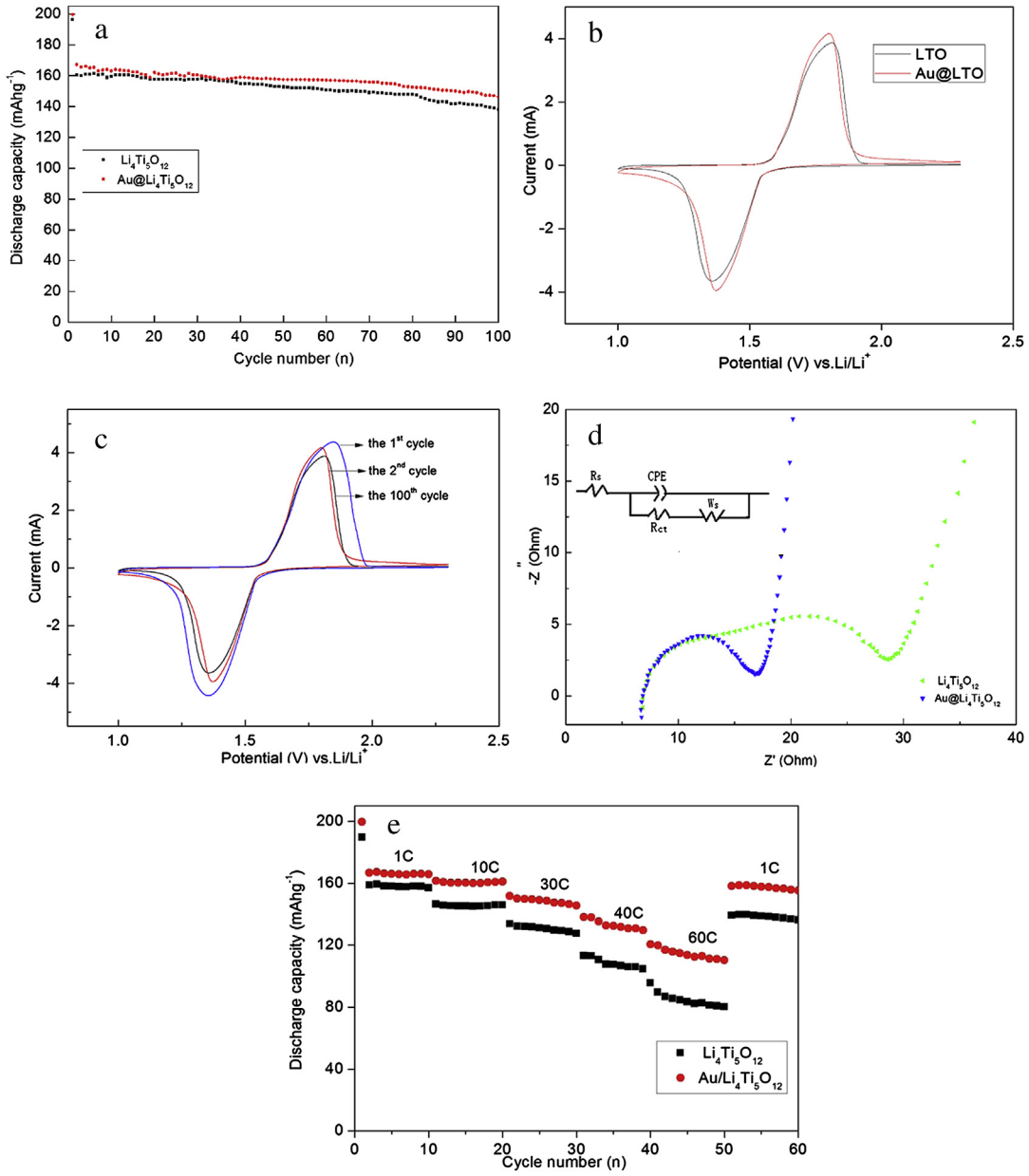

Fig. 4. (a) The cycling performance of bare $Li_4Ti_5O_{12}$ and Au@$Li_4Ti_5O_{12}$ measured at 5 C. (b) Cyclic voltammetry plots of bare $Li_4Ti_5O_{12}$ and Au@$Li_4Ti_5O_{12}$ bare $Li_4Ti_5O_{12}$ electrode at the scan rate of 0.05 mV $s^{-}1$. (c) The CV plots of the obtained Au@$Li_4Ti_5O_{12}$ electrode for the 1st, 2nd and 100th cycle. (d) The impedance spectra of are $Li_4Ti_5O_{12}$ and Au@$Li_4Ti_5O_{12}$ at the voltage of 1.55 V. The inset in Fig. 4d is the specific equivalent circuits. (e) The rate capabilities of bare $Li_4Ti_5O_{12}$ and Au@$Li_4Ti_5O_{12}$ measured at a series of current rates.

8.53×10^{-3} S cm^{-1}) is about a factor of ~10^9 higher than that of the pure $Li_4Ti_5O_{12}$ (ca. 10^{-13} S cm^{-1}), demonstrating the improved electron transport due to Au coating. The conductivities of the Au@$Li_4Ti_5O_{12}$ and $Li_4Ti_5O_{12}$ electrodes are evaluated from AC impedance spectroscopy at ambient temperature, and the typical Nyquist plots at the voltage of 1.55 V are given in Fig. 4d. The fitting results were obtained by ZView from Sai software set using an equivalent circuit, which is inset in Fig. 4d. In this equivalent circuit, R_s is the solution resistance. CPE is placed to represent the double layer capacitance and passivation film capacitance. The depressed semicircles at the high frequency side are reflective of charge transfer impedance (R_{ct}), which relates to the resistance of the electrode [15]. The R_{ct} of Au@$Li_4Ti_5O_{12}$ is 17 Ω, much lower than the 28 Ω of bare $Li_4Ti_5O_{12}$. The lithium ion diffusion coefficient (D_{Li}) is calculated according to the following equation [26,27]:

$$D_{Li} = \frac{(RT)^2}{2(An^2F^2C_{Li}\sigma)^2} \quad (1)$$

where n is the number of electrons per molecule during oxidization, A the surface area of the electrode, R the gas constant, T the absolute temperature, F the Faraday constant, C_{Li} the concentration of lithium ion, and s is the Warburg factor which has relationship with Z_{re}:

$$Z_{re} = R_{ct} + R_s + \sigma\omega^{-\frac{1}{2}} \quad (2)$$

Based on Eqs. (1) and (2), the lithium diffusion coefficients of Au@$Li_4Ti_5O_{12}$ is 7.32×10^{-10} cm^2 s^{-1}, much higher than the 3.18×10^{-10} cm^2 s^{-1} corresponding to bare $Li_4Ti_5O_{12}$. The optimum design of $Li_4Ti_5O_{12}$ nanorods with a uniform Au shell enables the fast

migration of both lithium ions and electrons to reach the interior of each active particle, enhancing the full utilization of the active materials. Fig. 4e exhibits the discharge capacities of bare $Li_4Ti_5O_{12}$ and Au@$Li_4Ti_5O_{12}$ electrode against different current rates from 1 C to 60 C, each sustained for 10 cycles. The stable cyclic performance of Au@$Li_4Ti_5O_{12}$ was obtained for all rates except 60 C. A specific capacity of ca. 155 mAh g^{-1} is recovered when the current rate reduced back to 1 C after 60 cycles at higher rates. The rate performance of resulting Au@$Li_4Ti_5O_{12}$ is much higher than that of pure $Li_4Ti_5O_{12}$ materials. Especially, the performance at such high rates is much better than that of nanoporous LTO [21,25], carbon-coated LTO [28], TiN-coated LTO [29] and TiO-LTO [30]. The overall rate performance data confirm again the importance of Au-coating toward high capacities in both low and high current rates. The superior cycling performance can be attributed to the unique nanorod characteristics, structural stability, and the improved ionic and electronic conduction in the electrode due to the nano coating of Au.

4. Conclusion

Applied of alcoholysis, solid-state reaction and coating techniques, Au@$Li_4Ti_5O_{12}$ nanorod aggregates materials are synthesized, and the diameter of the single nanorod is estimated to be 10–20 nm. The resulting Au@LTO materials possess high BET surface area of 50.35 $m^2\ g^{-1}$, and enhanced lithium diffusion coefficient of ca. 7.32×10^{-10} $cm^2\ s^{-1}$. The stable reversible capacity of electrode is 169 mAh g^{-1}, and can be retained at 154 mAh g^{-1} after 100 cycles with the retention of 91.1% at 5 C. The coulombic efficiencies are always over 99.3% except for the first cycle. Moreover, it also exhibits excellent rate-capability performance. The superior cycling performance can be attributed to the unique nanorod characteristics, structural stability, the improved ionic and electronic conduction in the electrode. These results demonstrate that Au@$Li_4Ti_5O_{12}$ composite material is a promising anode material for lithium-ion battery.

Acknowledgment

The authors would like to acknowledge financial support provided by Department Science Foundation of China (No. 210204), National Natural Science Foundation of China (No. U0937601) and 863 Program of National High Technology Research Development Project of China (No. 2011AA03A405).

References

[1] M. Armand, J.M. Tarascon, Nature 451 (2008) 652–657.
[2] A.K. Shukla1, T.P. Kumar, Curr. Sci. 94 (2008) 314–331.
[3] J.T. Han, Y.H. Huang, J.B. Goodenough, Chem. Mater. 23 (2011) 2027–2029.
[4] L. Aldon, P. Kubiak, M.C. Womes, J. Jumas, J. Olivier-Fourcade, J.L. Tirado, J.I. Corredor, C.P. Vicente, Chem. Mater. 16 (2004) 5721–5725.
[5] S.H. Huang, Z.Y. Wen, X.J. Zhu, Z.G. Gu, Electrochem. Commun. 6 (2004) 1093–1097.
[6] H. Ge, N. Li, D. Li, C. Dai, D. Wang, Electrochem. Commun. 10 (2008) 719–722.
[7] L. Cheng, J. Yan, G.N. Zhu, J.Y. Luo, C.X. Wang, Y.Y. Xia, J. Mater. Chem. 20 (2010) 595–602.
[8] M. Wagemaker, E.R.H. van Eck, A.P.M. Kentgens, F.M.J. Mulder, Phys. Chem. B 113 (2009) 224–230.
[9] S. Takai, M. Kamata, S. Fujine, K. Yoneda, K. Kanda, T. Esaka, Solid State Ionics 123 (1999) 165–172.
[10] C.H. Chen, J.T. Vaughey, A.N. Jansen, D.W. Dees, A.J. Kahaian, T. Goacher, M.M. Thackeray, J. Electrochem. Soc. 148 (2001) A102–A104.
[11] S.C. Lee, S.M. Lee, J.W. Lee, J.B. Lee, S.M. Lee, S.S. Han, H.C. Lee, H.J. Kim, J. Phys. Chem. C 113 (2009) 18420–18423.
[12] J.Z. Chen, L. Yang, S.H. Fang, Y.F. Tang, Electrochim. Acta 55 (2010) 6596–6600.
[13] H.G. Jung, S.T. Myung, C.S. Yoon, S.B. Son, K.H. Oh, K. Amine, B. Scrosati, Y.K. Sun, Energy Environ. Sci. 4 (2011) 1345–1351.
[14] M.M. Rahman, J.Z. Wang, M.F. Hassan, S.L. Chou, D. Wexler, H.K. Liu, J. Power Sources 195 (2010) 4297–4303.
[15] Y.F. Tang, L. Yang, Z. Qiu, J.S. Huang, Electrochem. Commun. 10 (2008) 1513–1516.
[16] M.R. Jo, K.M. Nam, Y.M. Lee, K. Song, J.T. Park, Y.M. Kang, Chem. Commun. 47 (2011) 11474–11476.
[17] S.H. Huang, Z.Y. Wen, X.L. Yang, Z.H. Gu, X.H. Xu, J. Power Sources 148 (2005) 72–77.
[18] S.H. Huang, Z.Y. Wen, J.C. Zhang, Z.H. Gu, X.H. Xu, Solid State Ionics 177 (2006) 851–855.
[19] Y. Amiki, F. Sagane, K. Yamamoto, T. Hirayama, M. Sudoh, M. Motoyama, Y. Iriyama, J. Power Sources (2013), http://dx.doi.org/10.1016/j.jpowsour.2013.05.006.
[20] J. Morales, R. Trócoli, E. Rodríguez-Castellón, S. Franger, J. Santos-Peña, J. Electroanal. Chem. 631 (2009) 29–35.
[21] C.C. Li, Q.H. Li, L.B. Chen, T.H. Wang, Appl. Mater. Interfaces 4 (2012) 1233–1238.
[22] N.Q. Zhang, Z.M. Liu, T.Y. Yang, C.L. Liao, Z.J. Wang, K.N. Sun, Electrochem. Commun. 13 (2011) 654–656.
[23] J.C. Arrebola, A. Caballero, M. Cruz, L. Hrenan, J. Morales, E.R. Castellon, Adv. Funct. Mater. 16 (2006) 1904–1912.
[24] C. Lai, Y.Y. Dou, X. Li, X.P. Gao, J. Power Sources 195 (2010) 3676–3679.
[25] L.F. Shen, C.Z. Yuan, H.J. Luo, X.G. Zhang, K. Xu, Y.Y. Xia, J. Mater. Chem. 20 (2010) 6998–7004.
[26] Q. Cao, H.P. Zhang, G.J. Wang, Q. Xia, Y.P. Wu, H.Q. Wu, Electrochem. Commun. 9 (2007) 1228–1232.
[27] A.Y. Shenouda, H.K. Liu, J. Power Sources 185 (2008) 1386–1391.
[28] G.N. Zhu, H.J. Liu, J.H. Zhuang, C.X. Wang, Y.G. Wang, Y.Y. Xia, Energy Environ. Sci. 4 (2011) 4016–4022.
[29] K.S. Park, A. Benayad, D.-J. Kang, S.-G. Doo, J. Am. Chem. Soc. 130 (2008) 14930–14931.
[30] Y.Q. Wang, L. Gu, Y.G. Guo, H. Li, X.Q. He, S. Tsukimoto, Y. Ikuhara, L.J. Wan, J. Am. Chem. Soc. 134 (2012) 7874–7879.